Optimized Synthetic Routes for Pd_3Se_{10}: A Superatomic Cluster Compound

Research Thesis

Presented in partial fulfillment of the requirements for graduation
with Research Distinction in Chemistry in the undergraduate
colleges of The Ohio State University

by

Chenguang Wang

The Ohio State University
May 2024

Project Advisor: Professor Joshua Goldberger, Department of Chemistry and Biochemistry

Table of Contents

Acknowledgements

First, I would like to thank Dr. Joshua Goldberger for providing me this opportunity to join his laboratory and participate in chemical research. This experience has not only expanded my knowledge in chemistry, but also improved my ability to conduct independent research. I also want to thank all members of the Goldberger group who make this lab well-operated and keep it a safe place to work. Among my labmates, I give my special thanks to Mr. Cullen Irvine, who took me under his mentorship and continuously guided me throughout this project, he showed me what characters a successful researcher should have through his actions. Most importantly, this research experience made me a prepared person to face challenges in my future academic career.

List of Figures and Tables

Abstract

Cluster-based compounds have attracted the attention of emergent materials design because of their stability, tunability, and functionality that can be used in materials design [**1**]. Here, we reported a newly discovered cluster compound – Pd_3Se_{10}, which is comprised of Pd_6Se_{20} cubes, with palladium (Pd) atoms located at 6 faces and selenium (Se) atoms located at the 12 edges and 8 corners. We have been able to successfully synthesize Pd_3Se_{10} through solution-phase reactions and established an electrochemically balanced route towards preparing high yields (76%) of material. The powder X-ray diffraction (PXRD) characterization showed that the resulting product is of high purity and large average crystal size (27.6 nm), and other Pd-Se phases are not present. The thermal gravimetric analysis and differential scanning calorimetry (TGA-DSC) shows there is a phase transition at 355°C, during which Pd_3Se_{10} decomposes to orthorhombic-$PdSe_2$ (o-$PdSe_2$). The diffuse reflectance accessory UV-vis (DRA UV-Vis) and diffuse reflectance infrared Fourier transformation spectroscopy (DRIFTS) results indicate that this material is a semiconductor with an indirect band gap of 1.16 eV. Overall, this work lays the foundation for the future investigation of this unique cluster into a broad range of applications.

Introduction

The discovery of C_{60} fullerene in 1985 opened the new world for materials chemical research because of its unique "buckeyball" structures consisted of clusters of 60 carbon atoms [**2**] and its properties like high T_c superconductivity (18~30 K) when doped with alkali metals [**3**, **4**, **5**]. Since then, research on cluster materials has prospered in number. Beyond C_{60}, more unique structures and properties have been discovered and studied. For example, gold nanoclusters [**Figure 1a-c**] and Chevrel phase compounds [**Figure 1d**] have flexible structures so that their electronic properties can be tuned by adding ligands and intercalating ions, which allows their applications in catalysis, electronics, and magnetic materials [**6**, **7**].

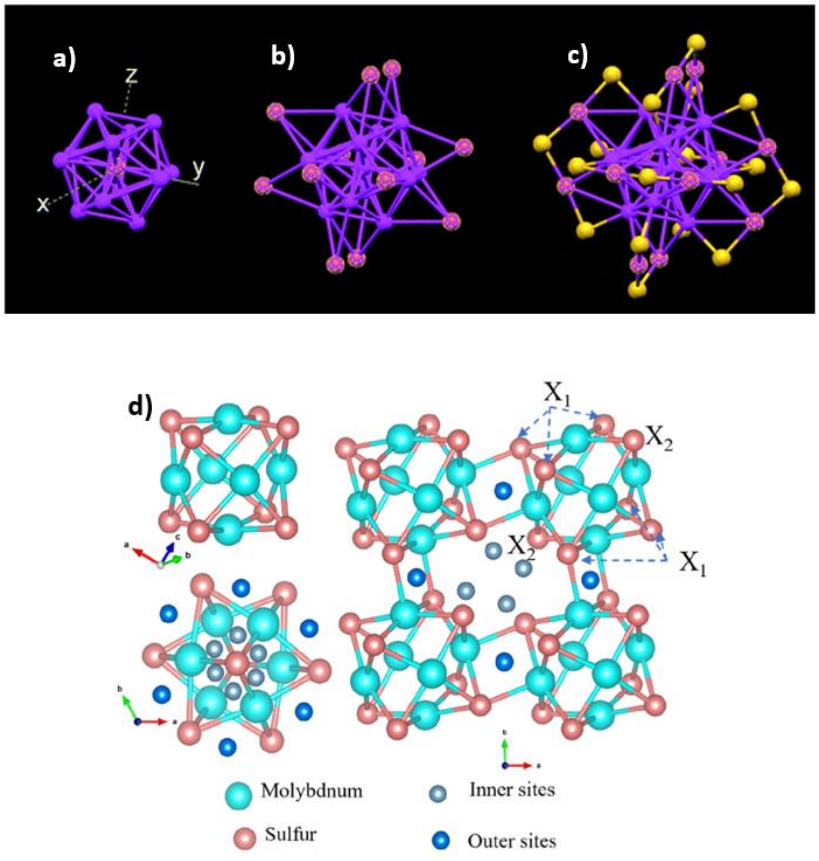

Figure 1. (**a**) Crystal structure of a Au_{13} icosahedral cluster. (**b**) Crystal structure of a Au_{25} cluster by capping a second shell of 12 Au atoms onto the Au_{13} cluster. (**c**) Crystal structure of a $Au_{25}(SR)_{18}$ cluster by capping a third shell of 18 -SR ligands onto the Au_{25} cluster [**Figure taken from ref. 6]** (**d**) Crystal structure of Chevrel phase Mo_6S_8, inner and outer sites are where ions can be intercalated into [**Figures taken from ref. 7**].

Besides serving as individual clusters with tunable properties, some clusters form atomically precise structures which give rise to collective properties mimicking those of traditional atoms, thus they are also called "superatoms" [**8**]. A larger family of materials can be obtained by assembling these superatoms through chemical reactions. Furthermore, these compounds will show new properties that are not possessed by any of those building blocks. One example is C_{60}-based superatomic crystals [**Figure 2a**], it shows a long-range ferromagnetic order below 4 K, but neither of the two building blocks behave as a ferromagnet [**Figure 2b**].

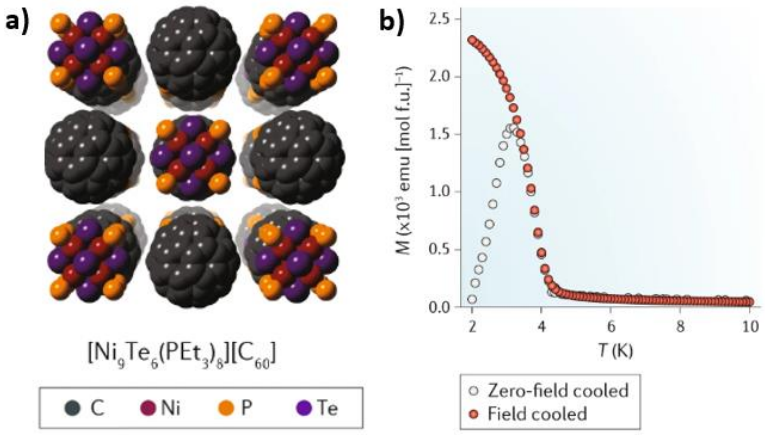

Figure 2. (a) Crystal structure of superatomic crystals $[Ni_9Te_6(Pet_3)_8]$ $[C_{60}]$. (**b**) Temperature dependence of the zero-field cooled and field cooled magnetization for $[Ni_9Te_6(PEt_3)_8]$ $[C_{60}]$ [**Figures taken from ref. 8**].

This project discusses a newly discovered cluster compound – Pd_3Se_{10}, whose structure resembles that of $AuTe_2Se_{4/3}$ [**9, Figure 3**], however, it features 6 less electrons per cluster. Factors influencing the synthesis of Pd_3Se_{10} were investigated, and several methods were utilized to exfoliate them into single clusters to test their potential to serve as building blocks for superatomic crystals.

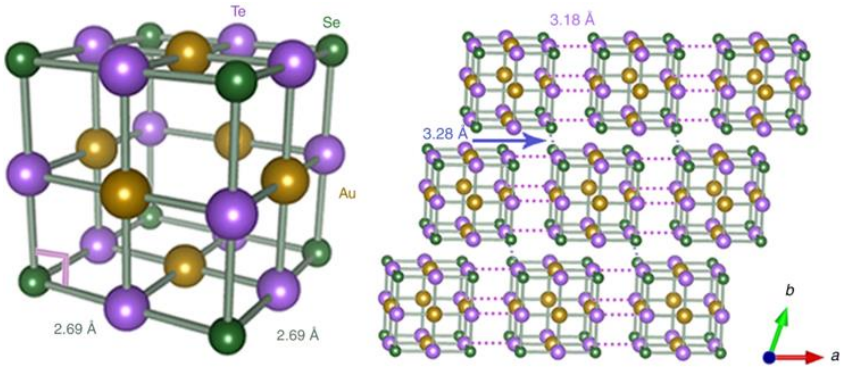

Figure 3. (Left) The structure of single block of atomically ordered Au-Te-Se. (Right) The structure of the ab-plane with two kinds of Te-Te bond lengths of 3.18 and 3.28 Å [**Figure taken from ref. 9**].

Synthesis and Characterization of the Se Precursor (Na_2Se_3)

$$NaBH_4 + 12Se + 7EtONa \xrightarrow[EtOH\ reflux]{1\ h} 4Na_2Se_3 + B(OEt)_3 + 4EtOH$$

Scheme 1. Chemical reaction equation for Na_2Se_3 synthesis.

The synthesis of Na_2Se_3 was modified from Yang *et al.* [**10**] by altering the amount of Se we added (**Scheme 1**). All reactions were conducted under argon atmosphere using Schlenk line technique. First, anhydrous ethanol (EtOH, 50 mL) was added into a flask containing sodium (Na, 0.3556 g, 15.47 mmol) to form sodium ethoxide (EtONa) in EtOH solution. Then, the EtONa solution was poured into a flask containing $NaBH_4$ (0.0836 g, 2.21 mmol), and more anhydrous EtOH (30 mL) was added to the flask. This solution was stirred to help $NaBH_4$ dissolve while the flask was put in an ice-water bath. Then the $NaBH_4$ solution was added to a three-neck flask containing Se powder (2.0936 g, 26.516 mmol) in anhydrous EtOH (10 mL). The resulting solution was stirred at room temperature, then heated to reflux and stirred for another 1 h. After the reaction was done, the solvent was removed, then the resulting powder was collected and grounded in the glovebox filled with argon. The powder was transferred to a new flask, the flask was then taken out of the glovebox,

connected to the Schlenk line, and put into a sand bath. The sand bath was heated to 200°C and the powder was annealed for 70 h under argon atmosphere. The flask was then taken back to the glovebox, and a black powder was collected and grounded. The powder was stored in a glass vial wrapped with aluminum foil.

Na_2Se_3 was characterized by X-ray Diffraction using Bruker D8 Advance Powder XRD (Cu $K\alpha_1$ radiation). The PXRD plate of air sensitive Na_2Se_3 powder was prepared in the glovebox and covered with Kapton tape. Using GSAS-II software, a Rietveld refinement was done on the PXRD result to determine the weight fractions of this "Na_2Se_3" product (**Figure 4)**. The relative ratio of Na:Se (2:3.37) was calculated (**Table 1**) and used for the reaction of Pd_3Se_{10} synthesis. Therefore, this Se precursor will be written as $Na_2Se_{3.37}$ for the rest of this thesis.

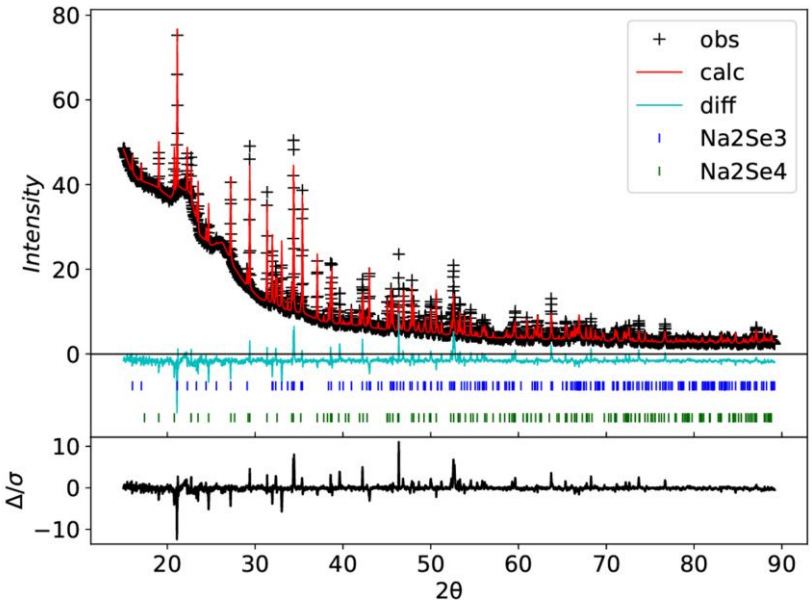

Figure 4. Rietveld refinement plot of the Se precursor using GSAS-II software. The observed data, calculated pattern, difference curve, *hkl* marks of Na_2Se_3, and *hkl* marks of Na_2Se_4 are shown with black crosses, red line, greenish blue line, blue line, and green line, respectively.

Chemical Formula	Na_2Se_3	Na_2Se_4
Formula Weight (g/mol)	282.86	361.82
Space Group	C2/c	$I\bar{4}2d$
Crystal System	Monoclinic	Tetragonal
a (Å)	11.2634(6)	10.1926(3)
b (Å)	4.2794(1)	N/A
c (Å)	10.5985(5)	12.2269(4)
β (°)	100.800(2)	N/A
Cell Volume ($Å^3$)	501.806	1270.247
Z	4	16
Density (g/mol)	3.7441	3.7840
Phase Fraction	0.763(4)	0.237(4)
Weight Fraction	0.557(6)	0.443(6)
Mole Fraction	0.616(5)	0.383(5)

Table 1. Crystal data and Rietveld refinement results from PXRD of the Se precursor, showing a molar ratio of Na_2Se_3 to Na_2Se_4 of 1.6:1.

Optimized Synthesis and Structural Characterization of Pd_3Se_{10}

Optimized Synthesis of Pd_3Se_{10}

$$3Na_2PdCl_4 + 2Na_2Se_3 + Na_2Se_4 \xrightarrow[\text{Triethylene glycol}]{200°C} Pd_3Se_{10} + 12NaCl$$

Scheme 2. Chemical reaction equation for Pd_3Se_{10} synthesis, which is balanced both stoichiometrically and electrochemically.

The idea of synthesizing Pd_3Se_{10} in triethylene glycol (TREG) was inspired by Li, *et al.* [**11**]. This synthetic route has been optimized to make Pd_3Se_{10} with high yield, purity, and crystallinity, and factors influencing the formation of Pd_3Se_{10} will be discussed separately. The optimized synthesis is shown below. In the glovebox, $Na_2Se_{3.37}$ (0.2090 g, 0.6696 mmol)) and Na_2PdCl_4 (0.1990 g, 0.6764 mmol) were measured and put into a three-neck flask and a glass vial (**Scheme 2**). The three-neck flask was connected the Schlenk line and filled with argon atmosphere. 45 mL of TREG was added to the flask, then it was stirred and heated to 200°C. At the same

time, 15 mL of TREG was added to the vial and heated to 60°C on a hot plate. Then the Na_2PdCl_4/TREG solution was injected to the Na_2Se_2/TREG solution using a syringe, at a rate of 0.5 mL/20 s over the course of 10 min. The temperature was kept at 200 ± 2°C during the injection. The reaction was ended by removing the heat from the flask, then it was air-cooled to room temperature. The resulting solution was centrifuged at 3000 rpm for 10 min, then the supernatant was decanted off, the solid left was then washed with DI water for 3 times and methanol for 2 times, each time a centrifuge at 3000 rpm for 5 min was performed. The final product was air-dried to yield black solid (0.1919 g, 76.77 %).

Structural Characterization of Pd_3Se_{10}

Pd_3Se_{10} was characterized by X-ray Diffraction using Bruker D8 Advance Powder XRD (Cu $K\alpha_1$ radiation). The dried product from above was broken into powder using a spatula, then it was loaded into a PXRD plate under ambient conditions. The result was shown below (**Figure 5a**). The Pd_3Se_{10} product was also characterized using high-angle annular dark-field scanning transmission electron microscopy (HAADF-STEM) and transmission electron microscopy (TEM) (**Figure 5a**), and the HAADF-STEM indicated the cubic Pd_3Se_{10} clusters (**Figure 5b**) [**12**].

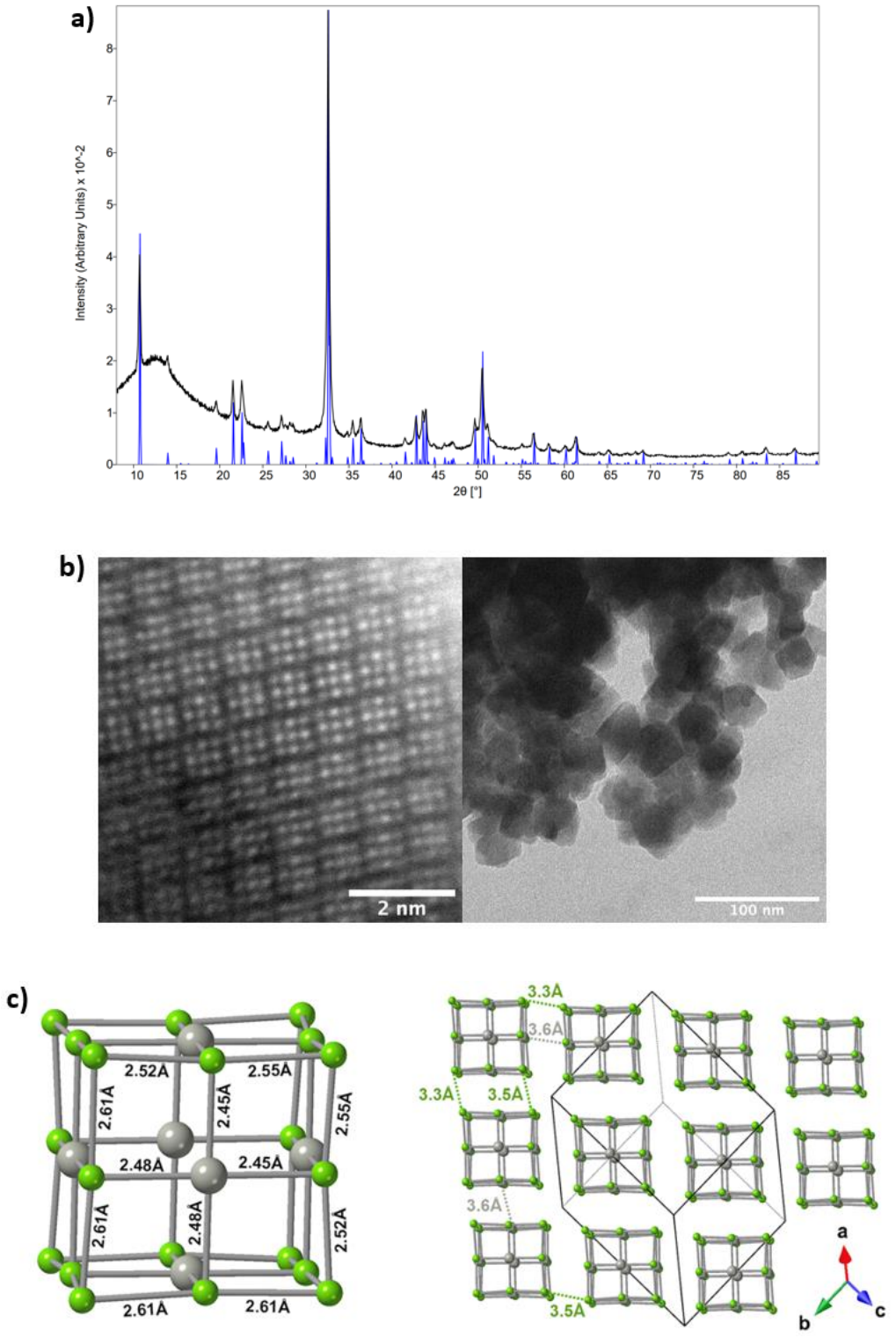

Figure 5. (**a**) PXRD pattern of Pd_3Se_{10} (black pattern) synthesized using the optimized route, where blues lines are Pd_3Se_{10} pattern from ICSD website. (**b**) (Left) HAADF-STEM and (right) TEM images of Pd_3Se_{10}, showing the cubic structure of Pd_3Se_{10} clusters. (**c**) (Left) The structure of a single block of atomically ordered Pd (grey)-Se (green). (Right) The crystal structure of Pd_3Se_{10}, where black lines represent the trigonal unit cell with Pd-Pd bond length of 3.6 Å and Se-Se bond lengths of 3.3 and 3.5 Å. [**Structural representation taken from ref. 12**]

Factors Influencing the formation of Pd_3Se_{10}

Syntheses of Pd_3Se_{10} were performed under different temperatures, times, and injection rates of Na_2PdCl_4 precursor. We found that the yield, purity, and crystallinity of Pd_3Se_{10} were highly dependent on these factors. In general, we will show that the samples with highest yield and largest crystalline domain sizes were grown at 200°C, and with an injection rate of 0.25 mL/min of the Na_2PdCl_4 precursor.

Temperature Dependence

Here we studied the influence of temperature on the formation of Pd_3Se_{10} phases. In three independent syntheses, the $Na_2Se_{3.37}$/TREG solution was heated to 100°C, 150°C, and 200°C, then the 60°C Na_2PdCl_4/TREG solution was poured into it. All reactions were kept at the temperature of the $Na_2Se_{3.37}$/TREG solution before the addition of the Pd precursor, then they were stopped after 10 min and air-cooled to room temperature. Other than these, all procedures were the same. We have found that to grow a crystalline Pd_3Se_{10} product, the temperature must be higher than 150°C. Below this temperature, the product is amorphous (**Figure 6a**). The three products grown at different temperatures were further characterized using Raman spectroscopy, and the results showed that all peaks line up with each other (**Figure 6b**). Apparently, all three products are Pd_3Se_{10}, and the only difference is the crystalline domain size or amorphous nature. To further confirm bonding characters in amorphous Pd_3Se_{10} products, Raman spectra were taken for other Pd/Se containing phases that are common impurities in Pd_3Se_{10} syntheses. Se sample was powder from Thermo Scientific (99.999%), o-$PdSe_2$ and monoclinic-$PdSe_2$ were prepared via solution methods reported in Irvine, *et al.* [**12**]. The results (**Figure 6c**) showed amorphous Pd_3Se_{10} do not match with other Pd/Se containing phases, which proved that

amorphous and crystalline Pd_3Se_{10} have the same bonding characters.

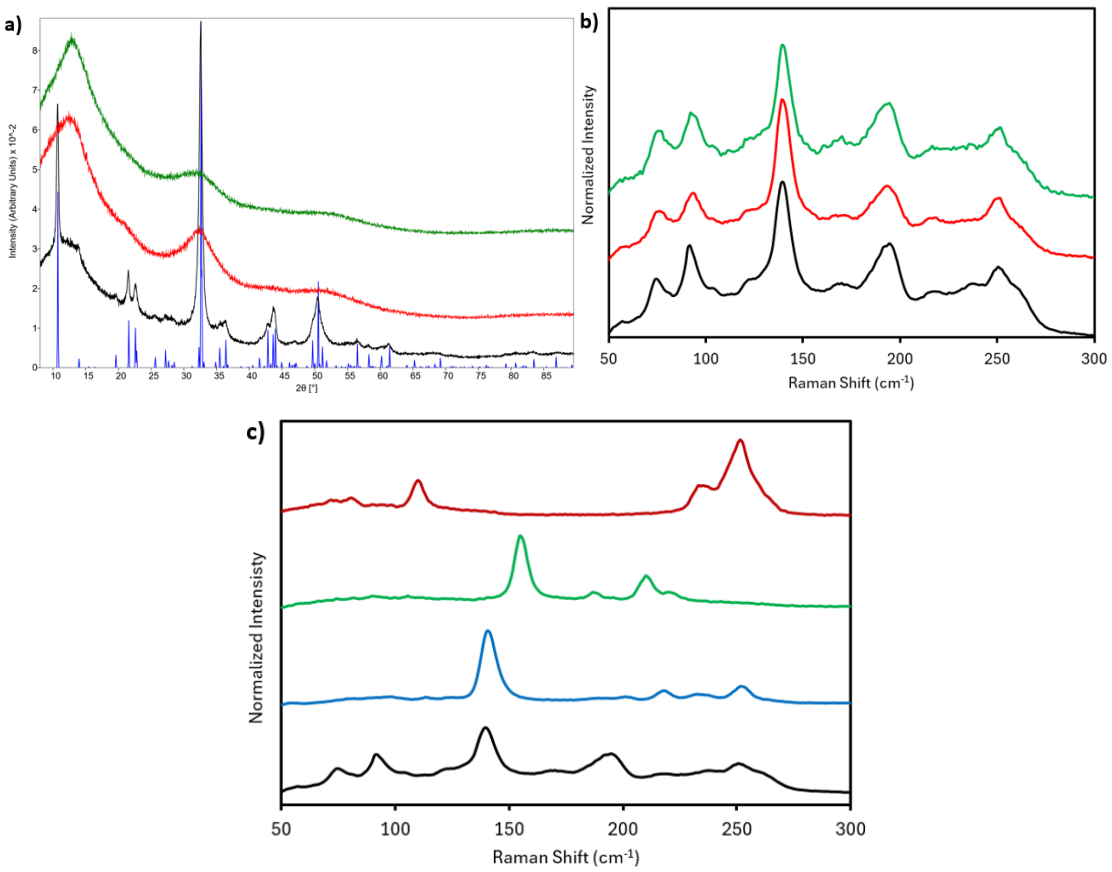

Figure 6. (**a**) PXRD patterns of Pd_3Se_{10} products from different reaction temperatures, comparing 100°C (green), 150°C (red), and 200°C (black). Blue lines are Pd_3Se_{10} pattern from ICSD website. (**b**) Raman spectra of Pd_3Se_{10} products from different reaction temperatures, comparing 100°C (green), 150°C (red), and 200°C (black). (**c**) Raman spectra of other Pd-Se phases, comparing Se (red), m-$PdSe_2$ (green), o-$PdSe_2$ (blue), and Pd_3Se_{10} (black).

Time Dependence

Here we studied the influence of reaction time on the formation of Pd_3Se_{10} phases. Na_2PdCl_4/TREG and $Na_2Se_{3.37}$/TREG solutions were heated to 60°C and 245°C, respectively, immediately after this, Na_2PdCl_4/TREG was poured into the $Na_2Se_{3.37}$/TREG, and the temperature dropped to 210°C. In three independent syntheses, the reactions were kept at 210 ± 2°C, then they were stopped after 30 s, 3 min, and 1 hr. Reactions were then cooled to room temperature in an ice-water bath. Other than these, all procedures were the same. We have found that to grow a phase

pure Pd_3Se_{10} product, the reaction time must be shorter than 3min, beyond which impurities like o-$PdSe_2$ would form (**Figure 7**). The formation of Pd_3Se_{10} and o-$PdSe_2$ will compete under this reaction condition. A short reaction time like 30 s is necessary to form phase pure Pd_3Se_{10}, otherwise o-$PdSe_2$ would become the dominant phase in the product.

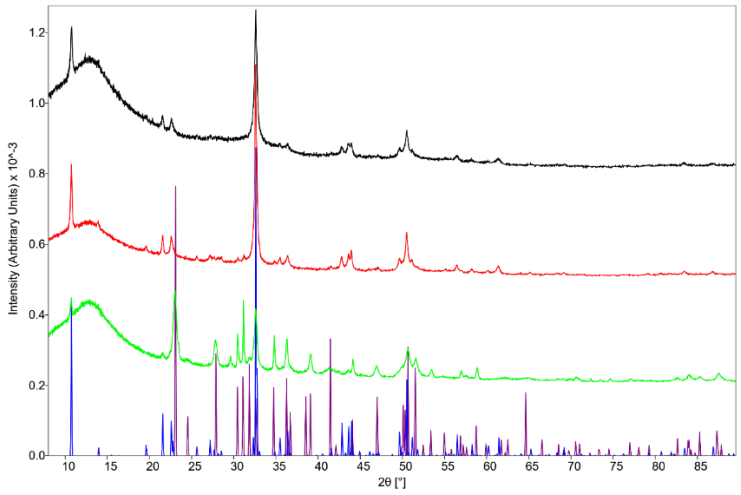

Figure 7. PXRD patterns of Pd_3Se_{10} products from different reaction times, comparing 30 s (black), 3min (red), and 1hr (green). Blue and purple lines are Pd_3Se_{10} and o-$PdSe_2$ patterns from ICSD website.

Injection Rate Dependence

Here we studied the influence of reaction time on the formation of Pd_3Se_{10} phases. This idea was inspired by Achon, *et al*. where they found that a slow injection rate of their phosphorus (P) precursor helped them form large and monodisperse InP quantum dots (**13**). Our synthetic process is shown below. Na_2PdCl_4/TREG and $Na_2Se_{3.37}$/TREG solutions were heated to 60°C and 200°C, respectively. Then, in three independent syntheses, Na_2PdCl_4/TREG was injected into $Na_2Se_{3.37}$/TREG in three different rates, which were fast pouring (over 3 s), 0.5 mL/20 s (over 10 min), and 0.25 mL/min (over 1 hr). For fast pouring, the reaction was stopped after 10 min; for slow injecting, reactions were stopped after all Na_2PdCl_4/TREG was injected. We have found

that a slow injection rate (either 0.5 mL/20 s or 0.25 mL/min) would help increase the crystal domain size of Pd_3Se_{10}, as indicated by a smaller FWHM of the peak at [3 0 3] (**Figure 8b**). The reaction could also run for longer without impurity formation (like o-$PdSe_2$) (**Figure 8a**).

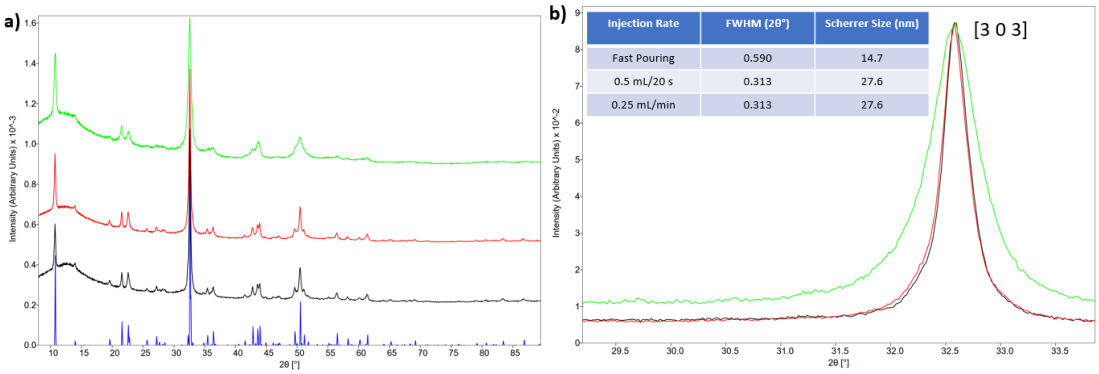

Figure 8. (**a**) PXRD patterns of Pd_3Se_{10} products from different injection rates, comparing the addition of Na_2PdCl_4/TREG over 3 s (green), 10 min (red), and 1 hr (black). Blue lines are Pd_3Se_{10} pattern from ICSD website. (**b**) Inset FWHM and Scherrer size comparison of PXRD pattern of Pd_3Se_{10} products from different injection rates, highlighting the [3 0 3] plane.

Property Study of Pd_3Se_{10}

Thermal Stability Testing

TGA was used to test the thermal stability of Pd_3Se_{10}. The TGA was set to perform from 25°C to 500°C, with a ramp rate of 10°C/min. The TGA result (**Figure 9a**) showed a mass loss and a heat transfer (endothermic) at 355°C. After TGA, PXRD analysis was performed on the product (**Figure 9b**), which showed that Pd_3Se_{10} decomposed into o-$PdSe_2$. Based on these results, the decomposition reaction of Pd_3Se_{10} was proposed (**Scheme 3**). **Table 2** shows mass data of Pd_3Se_{10} before and after TGA, using both calculation results from the scheme and the result from TGA, and it proves our hypothesis for the reaction scheme. The TGA result also supports our synthetic method chosen for Pd_3Se_{10}, where the reaction took place in TREG solution and the temperature was kept at 200°C, which is lower than the boiling point

of TREG (285°C) and the decomposition temperature of Pd_3Se_{10}. The TGA results also showed that Pd_3Se_{10} is a phase competing with o-$PdSe_2$, which proved that Pd_3Se_{10} is the kinetic product and less stable than thermodynamic product o-$PdSe_2$.

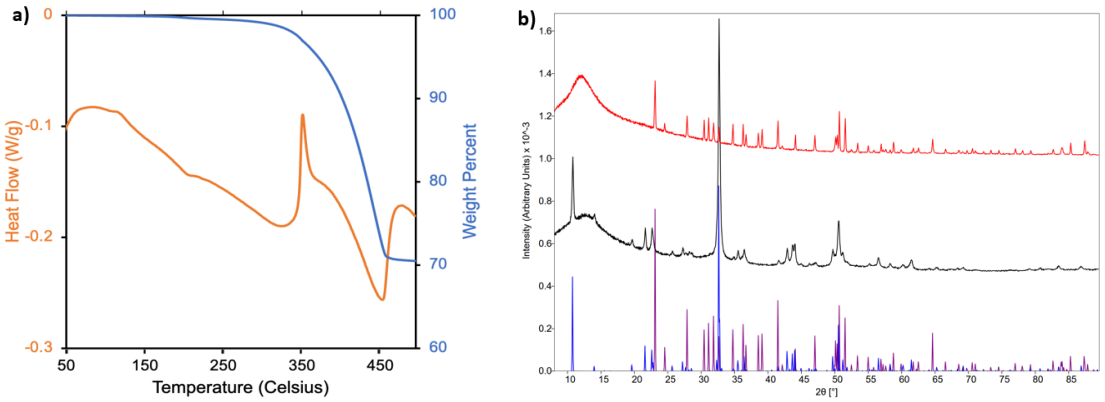

Figure 9. (**a**) TGA (blue) and DSC (orange) data of Pd_3Se_{10} product. (**b**) PXRD patterns of Pd_3Se_{10} product before (black) and after (red) TGA. Blue and purple lines are Pd_3Se_{10} and o-$PdSe_2$ patterns from ICSD website.

$$Pd_3Se_{10} \xrightarrow[355°C]{} 3PdSe_2 + 4Se$$

Scheme 3. Proposed Pd_3Se_{10} decomposition reaction based on TGA-DSC and PXRD, showing the decomposed product $PdSe_2$ and volatile Se.

Pd_3Se_{10} sample mass (assuming 100 g)	Before decomposition	After decomposition
Theoretical calculation	100 g	71.52 g
TGA results	100 g	70.48 g

Table 2. Calculated and experimental results of residue's mass before and after Pd_3Se_{10} decomposition.

DRA and DRIFTS measurements for Pd_3Se_{10}

To study the optical properties of Pd_3Se_{10}, DRA-UV-vis and DRIFTS were used to analyze Pd_3Se_{10}. For DRA measurement, a sample of Pd_3Se_{10} was grounded and mixed with dry KBr, the weight percent of Pd_3Se_{10} sample was 20% of the total. Then the powder was placed into a sample holder and taken a solid-state UV-vis from

2500 nm to 250 nm. For DRIFTS measurement, a sample of Pd_3Se_{10} was grounded into powder and placed into a sample holder, then it was taken DRIFTS from 8000 cm^{-1} to 400 cm^{-1}. Based on Makula *et al.* [**14**], the Tauc plot can be used to determine the band gap of semiconductors. This method assumes that the energy-dependent absorption coefficient α can be expressed by **Equation 1**. The γ factor is dependent on the nature of the electron transition and is equal to 1/2 or 2 for the direct and indirect band gaps. The band gap is determined using diffuse reflectance spectra. P. Kubelka, and F. Munk presented a theory that converts measured reflectance to the corresponding absorbance by applying **Equation 2**. Substituting α with F(R), the Tauc plot can be generated using **Equation 3**. The plot region showing a linear increase is characteristic of semiconductor materials and the intersection of this linear region and the onset linear region gives an estimate of the band gap energy. By applying this method, an indirect band gap of 1.16 eV for Pd_3Se_{10} was calculated, indicating its semiconducting property.

$$(\alpha * h\nu)^{1/\gamma} = B\,(h\nu - E_g)$$

Equation 1. The expression of energy coefficient α, where hν is the photon energy, E_g is the band gap, and B is a constant.

$$F(R) = \frac{(1-R)^2}{2R}$$

Equation 2. The Kubelka-Munk function, where R is the reflectance of an infinitely thick specimen, which is substituted by reflectance from DRA spectra.

$$(F(R) * h\nu)^{1/\gamma} = B\,(h\nu - E_g)$$

Equation 3. Substituting α in equation1 with F(R) gives this form, and the Tauc plot is based on this expression.

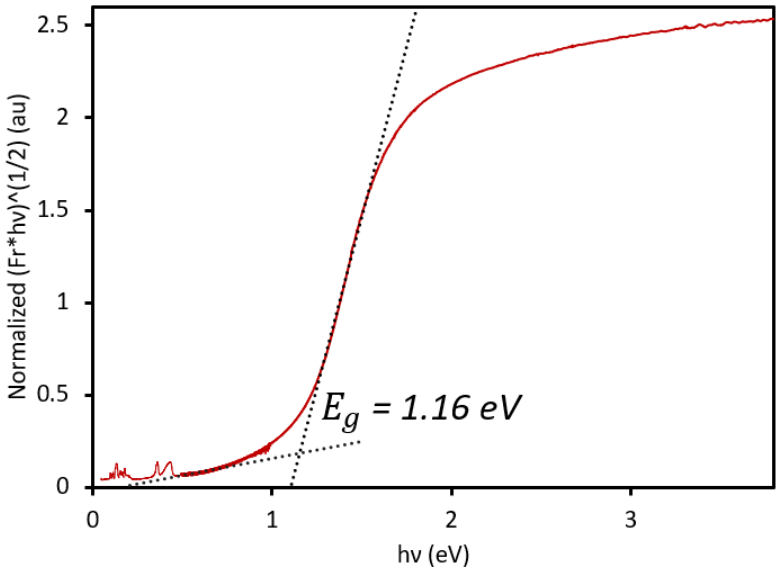

Figure 10. Tauc plot for determining the indirect band gap of Pd_3Se_{10} by combining DRA-UV-vis and DRFITS spectra (red line) and fitted lines from the linear regions (dashed lines).

Exfoliation of Pd_3Se_{10}

To test the potential of Pd_3Se_{10} to serve as building blocks for materials design, we tested different methods to exfoliate Pd_3Se_{10} into single clusters. Two methods were reported here, which are ultrasonication and solvothermal process.

Ultrasonication

Ultrasonication was previously used to assist the dispersion of carbon nanotubes (CNTs) in a paper by Kharissova, *et al.* [**15**], where a probe-type ultrasonication method was used to disperse CNTs in methanol, without applying surfactants. Thus, we explored using this ultrasonication method to disperse Pd_3Se_{10} in various solvents (DI H_2O, NMF, and DMF). First, Pd_3Se_{10} powder (5 mg) was weighed out and put into centrifuge tubes containing 30 mL of these solvents. To better disperse Pd_3Se_{10}, we added surfactants like SDS, PVP, and sodium cholate. **Figure 11a** shows a conventional ultrasonication set up [**16**]. In our experiments, a

probe-type ultrasonicator was used to disperse Pd_3Se_{10} in these solvents, and the total sonication time was set to be 1h. To prevent over-heating of the solution and the probe, the centrifuge tube was submerged in an ice bath and the ultrasonicator was set to run for 40 s and stop for 20 s. After 1 h, the solution was centrifuged at 3000 rpm for 10 min, the supernatant was then centrifuged at 12000 rpm for another 10 min. The second supernatant was taken a UV-vis analysis from 1400 nm to 200 nm. The goal was to see an absorption peak below 1072 nm because Pd_3Se_{10} has an indirect band gap of 1.16 eV. Unfortunately, none of these solvents or surfactants worked, even after increasing ultrasonication time or reducing the concentration of Pd_3Se_{10} in these solvents. The UV-vis results didn't show absorption peaks below 1072 nm. (**Figure 11b**).

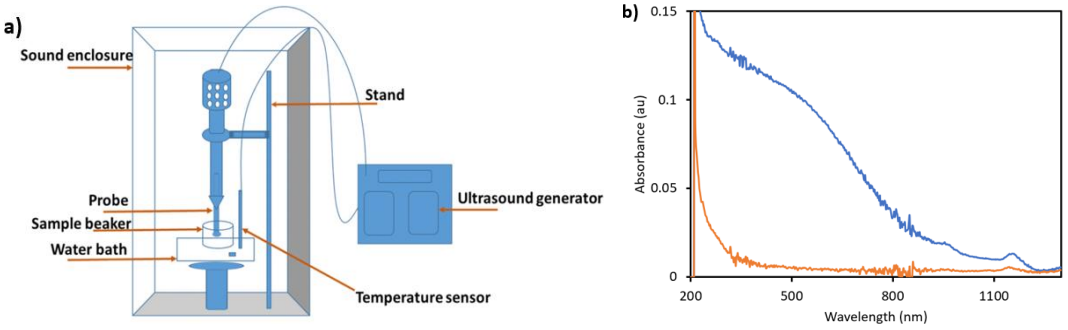

Figure 11. (**a**) Schematic drawing of a probe-type ultrasonication set up [**Figure taken from ref. 16**]. (**b**) UV-vis spectra from supernatant after ultrasonication and centrifugation at 3000 rpm (blue) and 12000 rpm (orange).

Solvothermal process

A solvothermal-assisted liquid exfoliation of boronphene was reported in Zhang *et al*., [**17**]. In this paper, few-layer borophene were obtained through a solvothermal process, followed by sonication and centrifuge. They used acetone, DMF, acetonitrile, ethanol, and NMP as their solvents and put boron powders in them, then they put them into Parr bombs. By heating this Parr bombs to 200°C, the

pressure inside them became more than 20 MPa. As described in this paper, they were able to get few-layer borophene after this. To exfoliate few-layer borophene, one would need to break those strong B-B bonds between the layers. We interpreted the idea of breaking strong bonds in bulk boron and thought that the solvothermal process could help break the strong interactions among Pd_6Se_{20} cubes, therefore single clusters could be obtained. In our experiments, Pd_3Se_{10} powder (~1 mg) was measured and put into a glass vial, then the solvent (we tried DI H_2O, acetone, acetonitrile, and DMF) was added to the vial. The vial was then sonicated for 5 min to disperse Pd_3Se_{10} into the solvent. Then the solvent containing Pd_3Se_{10} was transferred to a Teflon cup, and the cup was put into a Parr bomb and sealed tightly. (**Figure 12** [**18**] shows what a Parr bomb looks like and names of its components, our Parr bombs look different that this one but has same components).

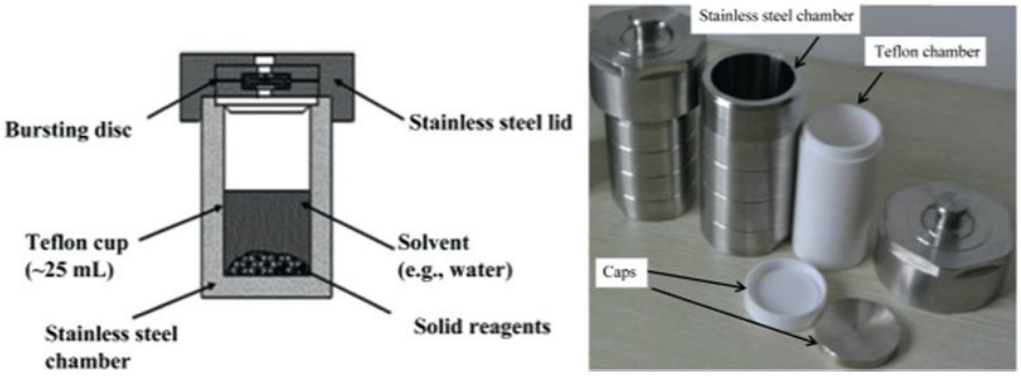

Figure 12. (Left) Cross section of a Parr bomb, where Pd_3Se_{10} and solvents were put inside the Teflon cup. (Right) Different parts of a Parr bomb [**Figures taken from ref. 18**].

Then the Parr bomb was put into a furnace, then it was heated to 200°C and reacted for 24h. After this, the liquid was taken out and centrifuged at 3000 rpm for 5 min. The supernatant was taken a UV-vis from 2000 nm to 190 nm. In our four solvent-trails, the color of the liquid after solvothermal reaction was orange for acetone, yellow for DMF, and pale-yellow for DI H_2O and acetonitrile (**Figure 13a**).

Specifically for DI H_2O results, a peak at 258 nm was observed and its intensity reduced as the supernatant was diluted (**Figure 13b**). However, no Pd-containing phases were observed in electrospray ionization mass spectrometry (ESI-MS) making detailed confirmation challenging.

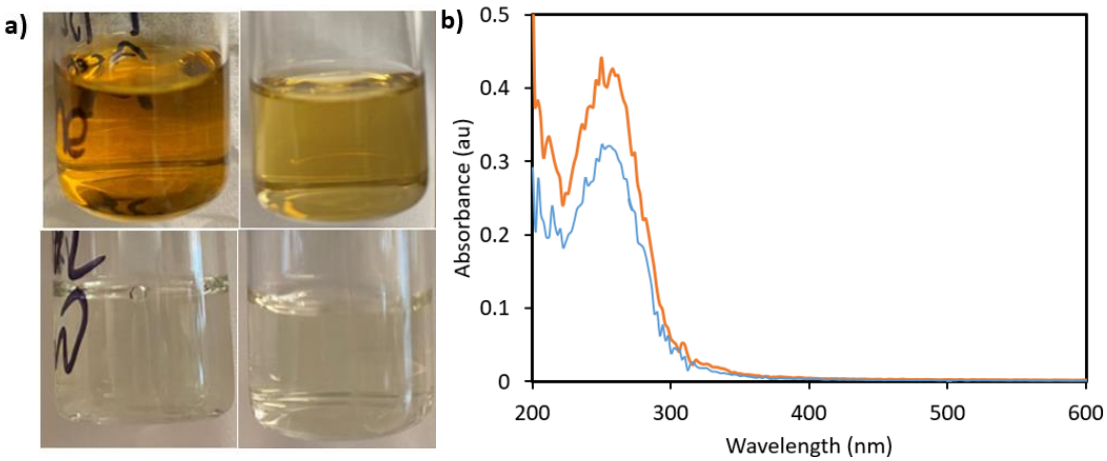

Figure 13. (**a**) Resulting solutions after solvothermal reactions in different solvents (left to right: top two: acetone, DMF; bottom two: DI H_2O, acetonitrile). (**b**) UV-vis spectra of supernatant after solvothermal reaction in DI H_2O, diluted by the factor of 20 (orange) and 40 (blue).

Conclusion and Future Work

A reproducible synthetic route for Pd_3Se_{10} has been established to produce a phase-pure and highly crystalline product, where the yield, purity, and crystallinity of Pd_3Se_{10} are maximized when the synthesis takes place at 200°C, during which Na_2PdCl_4 precursor is slowly injected into $Na_2Se_{3.37}$ precursor. The optical measurements showed its semiconducting property with an indirect band gap of 1.16 eV, which indicates its potential in applications in electronics and optoelectronics. Unlike traditional solid-state synthesis, the formation of Pd_3Se_{10} occurred at mild conditions, the time dependence results and TGA experiment showed that Pd_3Se_{10} is a meta-stable phase and it competes with the more thermodynamically stable o-$PdSe_2$ product. For future work, the exfoliation of Pd_3Se_{10} can be further studied using other

methods, and we believe it is important in order to test its potential to serve as superatomic building blocks for inorganic materials. To conclude, being able to reproducibly prepare highly pure and crystalline Pd_3Se_{10} opens the door of this new family of superatomic cluster materials.

References

1. S. A. Claridge, A. W. Castleman Jr., S. N. Khanna, C B. Murray, A. Sen, & P. S. Weiss, *ACS Nano*, **2009**, 3 (2), 244-255.
2. H. W. Kroto, J. R. Heath, S. C. O'Brien, R. F. Curl & R. E. Smalley, *Nature*, **1985**, 318, 162–163.
3. A. F. Hebard, M. J. Rosseinsky, R. C. Haddon, D. W. Murphy, S. H. Glarum, T. T. M. Palstra, A. P. Ramirez & A. R. Kortan, *Nature* **1991**, 350, 600–601.
4. K. Tanigaki, T. W. Ebbesen, S. Saito, J. Mizuki, J. S. Tsai, Y. Kubo & S. Kuroshima, *Nature* **1991**, 352, 222–223.
5. S. P. Kelty, CC. Chen & C. M. Lieber, *Nature* **1991**, 352, 223–225.
6. R. Jin, *Nanoscale*, **2010**, 2, 343-362.
7. M. Liu, G. Lv, T. Liu, H. Liu, L. Kong, L. Tian, W. Rao, Y. Li, L. Liao & J. Guo, *Prog. Nat. Sci. Mater*., 33 (**2023**), pp. 8-15.
8. E. A. Doud, A. Voevodin, T. J. Hochuli, A. M. Champsaur, C. Nuckolls & X. Roy, *Nat Rev Mater*, **2020**, 5, 371–387.
9. J. G. Guo, X. Chen, X. Y. Jia, Q. H. Zhang, N. Liu, H. C. Lei, S. Y. Li, L. Gu, S. F. Jin & X. L. Chen, *Nat Commun*, **2017**, 8, 871.
10. X. Yang, Q. Wang, Y. Tao and H. Xu, *J. Chem. Research (S)*, **2002**, 160–161.
11. J. Li, Z. Jin, T. Liu, J. Wang, X. Zheng & J. Lai, *CrystEngComm*, **2014**, 16, 6819-6822.
12. C. T. Irvine, N. Hoefer, M. J. Moser, R. A. Nelson, D. W. McComb, and J. E. Goldberger, *Chemistry of Materials*, **2023**, 35 (11), 4404-441.
13. O. B. Achorn, D. Franke & M. G. Bawendi, *Chemistry of Materials*, **2020**, 32 (15), 6532-6539.
14. P. Makuła, M. Pacia, and W. Macyk, *The Journal of Physical Chemistry*

Letters, **2018**, *9* (23), 6814-6817.

15. V. Kharissova, B. I. Kharisov and E. G. de C. Ortiz, *RSC Adv.*, **2013**, 3, 24812.
16. K. Desai, S. A. Dharaskar, M. Khalid, and T. Gupta, *Evironmental Science and Pollution Research*, **2021**, 28.
17. F. Zhang, L. She, C. Jia, X. He, Q. Li, J. Sun, Z. Lei, and Z. Liu, *RSC Adv.*, **2020**, 10, 27532.
18. R. Nagpal, M. Gusain, "Synthesis methods of quantom dots", Graphene, Nanotubes and Quantum Dots-Based Nanotechnology, edited by Yarub AI-Douri, *Woodhead*, **2022**, 599-630.